Macromolecular Materials and Engineering
Open Access
www.mame-journal.de

An Intriguing Array of Extrudate Patterns in Long-Chain Branched Polymers During Extrusion

*Sajjad Pashazadeh, Alexandra Aulova, Christos K. Georgantopoulos, Marko Bek, Iakovos Vittorias, Ingo F.C. Naue, Manfred Wilhelm, and Roland Kádár**

The present study highlights a range of surface and volume extrudate patterns that can be detected during the extrusion flow of long-chain branched polymers. Thus, four linear low-density polyethylenes (LDPEs) have been extruded using a single-screw extruder coupled to an inline optical imaging system. The selected LDPEs are selected to outline the influence of molecular weight and long-chain branching on the types of melt flow extrusion instabilities (MFEI). Through the inline imaging system, space–time diagrams are constructed and analyzed via Fourier-transformation using a custom moving window procedure. Based on the number of characteristic frequencies, peak broadness, and whether they are surface or volume distortions, three main MFEI types, distinct from those typically observed in linear and short-chain branched polymers, are identified. The higher molecular weight, low long-chain branching LDPEs exhibited all three instability types, including a special type volume instability. Independently of the molecular weight, higher long-chain branching appeared to have a stabilizing effect on the transition sequences by suppressing volume extrudate distortions or limiting surface patters to a form of weak intensity type.

1. Introduction

Sharkskin, stick-slip, and gross melt fracture are the main types of polymer melt flow extrusion instabilities (MFEI[1]), all being forms of surface or volume distortions induced in plastics during their extrusion.[2–7] Implicitly, this means that most studies have focused on linear and short-chain branched polymers for the study of MFEI, where such MFEI are prevalent and significant for the processing of polymers into products.[7] Especially sharkskin has been the subject of numerous studies focusing on its mitigation and control[8] and has driven significant innovations in inline measurement and detection systems.[9–16] In contrast, polymers with long-chain branched (LCB) topology, the most common example thereof being low-density polyethylene (LDPE), have been relatively overlooked from MFEI point of view. Some of the early focus on LCB polymers in the context of MFEI has been in relation to competing theories about the origin of MFEI in linear and/or short-chain branched. In addition, at the time there was conflicting evidence on the occurrence of pressure oscillations inside the die during the extrusion of LCB polymers.[17] In this context, Perez-Gonzalez et al.[17] showed that despite the absence of slip and a monotonic flow curve, pressure oscillations, having at least two characteristic frequencies, could be detected during the (capillary) extrusion of LDPE. Accordingly, their extrudates clearly showed evidence of both surface and volume MFEI. At around the same time, a branched polybutadiene, selected for birefringence visualizations, was reported to show surface cracks at the die exit, that is, sharkskin.[18] Delgadillo-Velázquez and Hatzikiriakos, (2007) investigated MFEI in LLDPE/LDPE blends. Pressure oscillations associated to the stick-slip instability were diminished with increasing LDPE weight fraction until it could no longer be detected (50 wt% LDPE).[19] Above 50%, sharkskin was also eliminated from the surface of the (cylindrical) extrudates[19] leaving only gross melt fracture as MFEI. It had been also inferred that because the presence of LCB increases the melt strength of the polymer, it should therefore mitigate the onset of the sharkskin instability. However, Yoo et al.[20] reported the opposite effect on a series of sparsely (less than two LCBs per 10^4 main chain carbons) long-chain branched metallocene linear low-density polyethylene (mLLDPE).[20] The surface patterns (cylindrical extrudates) identified included sharkskin and at

S. Pashazadeh, A. Aulova, M. Bek, R. Kádár
Department of Industrial and Materials Science
Chalmers University of Technology
Göteborg 41296, Sweden
E-mail: roland.kadar@chalmers.se
C. K. Georgantopoulos
Core Technology, Material and Manufacturing Technology
VAT Vakuumventile AG
Seelistrasse 1, Haag 9469, Switzerland
I. Vittorias
Technical Services Polymers
Baslerstrasse 42, Oftringen CH-4655, Switzerland
I. F. Naue, M. Wilhelm
Institute of Chemical Technology and Polymer Chemistry (ITCP)
Karlsruhe Institute of Technology (KIT)
Engesserstraße 18, 76131 Karlsruhe, Germany

The ORCID identification number(s) for the author(s) of this article can be found under https://doi.org/10.1002/mame.202300088

© 2023 The Authors. Macromolecular Materials and Engineering published by Wiley-VCH GmbH. This is an open access article under the terms of the Creative Commons Attribution License, which permits use, distribution and reproduction in any medium, provided the original work is properly cited.

DOI: 10.1002/mame.202300088

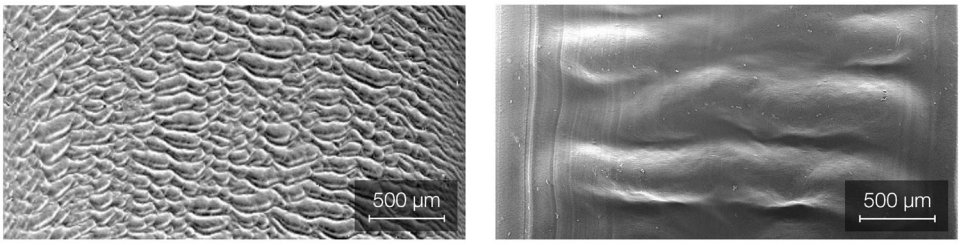

(a) (b)

Figure 1. Scanning electron microscopy (SEM) images comparing extrudates with a) typical sharkskin MFEI in a linear low-density polyethylene (LLDPE) and b) typical extrudate patterns in a low-density polyethylene (LDPE). Both visualizations were performed on extrudates from Georgantopoulos et al.[24]).

higher shear rates gross melt fracture.[20] Filipe et al.,[21] using an emerging state-of-the-art high-sensitivity piezoelectric pressure measurement system, included several LCB polymers in their study and reported surface and volume MFEI in some that they identified as sharkskin and stick-slip.[21] Gross melt fracture was reported as the main instability by Palza et al.[22] in a LCB-PE using an upgraded version of the high sensitivity die,[22] later commercialized by Goettfert GmbH. Burghelea et al.[23] compared an LLDPE with an LDPE during extrusion with a focus on in situ velocity distributions as revealed by laser Doppler velocimetry (LDV). They reported the LDPE extrudates as "stable" (no sharkskin) while showing the absence of slip at the die exit. In contrast, Kádár et al.[12] reported surface and volume instabilities in LDPE.[12] The results emphasized two surface patterns, one at lower shear rates defined by one characteristic frequency (based on in situ presure data) that then transitioned into a volume instability having two characteristic frequencies.[12] Without naming the MFEI types, the authors suggested based on the visual appearance of the extrudate distortions that they were not sharkskin. Interestingly, the characteristic frequencies associated to the detected MFEI in the LDPE studied were detected only in the transducers positioned at the die exit, suggesting the die exit as their origin. Recently, Georgantopoulos et al.[24] revisited the same LLDPE and LDPE polymers investigated by Burghelea et al.,[23] using a high sensitivity instability detection die and optical image analysis. The LDPE investigated in their study[24] has a very similar MFEI spectral behavior as reported by Kádár et al.[12]

Overall, there appear to be several perspectives when trying to define a particular MFEI. In one instance, a particular type of surface extrudate distortion can be associated to a particular type of MFEI based on its phenomenological origins. An example of such an approach would be associating sharkskin to the existence of slip at the die exit (no slip, no sharkskin).[17,23] A similar reasoning can be made based on whether the polymers show monotonic or non-monotonic flow curves[25] or whether the balance of tensile and shear stresses at the die exit in the presence of swelling can be linked to surface cracks. Complementary, geometrical arguments can be used to distinguish between surface and volume distortions based on how the amplitude of the extrudate distortions compare to the extrudate height, in the case of slit dies.[26] The development of in situ pressure systems capable of detecting pressure oscillations down to 10^{-3} bar made sharkskin instability detectable[10,11] and thus opened up the possibility of categorizing all instability types by considering the magnitude of the characteristic frequency of the instabilities.[16,21,22,27] In this respect, the characteristic frequency of primary instability (meaning MFEI that occurs first with increasing shear rate) in LDPE is typically one order of magnitude lower compared to sharkskin instability at their respective onset.[12,24] Furthermore, the visual appearance of the instabilities can be directly considered in order to distinguish MFEI. Such an example can be seen in **Figure 1** comparing SEM visualizations of instabilities in LLDPE and a LDPE: the two simply do not look the same. While sharkskin usually appears as a series of small interconnected surface cracks, LDPE surface distortions not only have a higher wavelength, they also usually span nearly the entire extrudate width in slit die extrusion.

Based on the considerations above, the present paper is written conceptually on the general hypothesis that MFEI extrudate patterns are very sensitive to the molecular properties of the extruded polymers.[18,28–30] Therefore, the main goal of the work is to identify distinct MFEI surface patterns in relation to the molecular and rheological properties of the polymer melts based on their visual appearance and associate spectral characteristics. In this context, we focus exclusively on long-chain branched polymers during single-screw extrusion characterized via inline optical imaging spectral analysis for the first time. Four linear low-density polymers (LDPEs) are tested to explore the influence of both molecular weight and long-chain branching. While generally neglected, long-chain branched polymers can show a rather intriguing array of surface and volume melt flow instabilities.

2. Materials, Characterization, and Processing

2.1. Materials

Four commercial (tubular) LDPEs (LDPE1-4) generously provided by LyondellBasell were used in this study.

In tubular LDPEs for the same melt flow rate (MFR) a decrease in density (ρ) generally signals more long-chain branching. Thus, based on the manufacturer specifications, see **Table 1**, pairs (LDPE3-LDPE4) are low MFR and pair (LDPE1-LDPE2) has the same, higher, MFR. While there is a factor of two difference in MFR between LDPE1 and LDPE2, the difference in MFR compared to the (LDPE3–LDPE4) pair is a factor of at least three. Meanwhile pairs (LDPE1–LDPE3) and (LDPE2–LDPE4) have the same densities, with the density increasing from the latter to the former pair. A bubble-chart of the four polymers in relation to both ρ and M_w can be found in **Figure 2**, where the size of the bubbles represents the polydispersity index, PDI. Therefore, the

© 2023 The Authors. Macromolecular Materials and Engineering published by Wiley-VCH GmbH

14392054, 0, Downloaded from https://onlinelibrary.wiley.com/doi/10.1002/mame.202300088 by Karlsruher Inst F. Technologie, Wiley Online Library on [06/07/2023]. See the Terms and Conditions (https://onlinelibrary.wiley.com/terms-and-conditions) on Wiley Online Library for rules of use; OA articles are governed by the applicable Creative Commons License

Table 1. Summary of the samples used in the study. Notations: ρ - density, MFR - melt flow rate (190 °C/2.16 kg), τ - relaxation time (as the inverse angular frequency at moduli crossover, please see Section 3), M_w and M_n are weight and number average molecular weights and PDI refers to polydispersity index.

Polymer	ρ [g cm^{-3}]	MFR [g/10 min]	τ [s]	M_w [g mol^{-1}]	M_n [g mol^{-1}]	PDI [-]
LDPE1	0.918	1.5	0.65	259 625	29 827	8.7
LDPE2	0.924	0.75	1.53	240 390	33 276	7.2
LDPE3	0.918	0.25	6.54	350 487	37 147	9.4
LDPE4	0.924	0.25	12.9	294 073	44 079	6.7

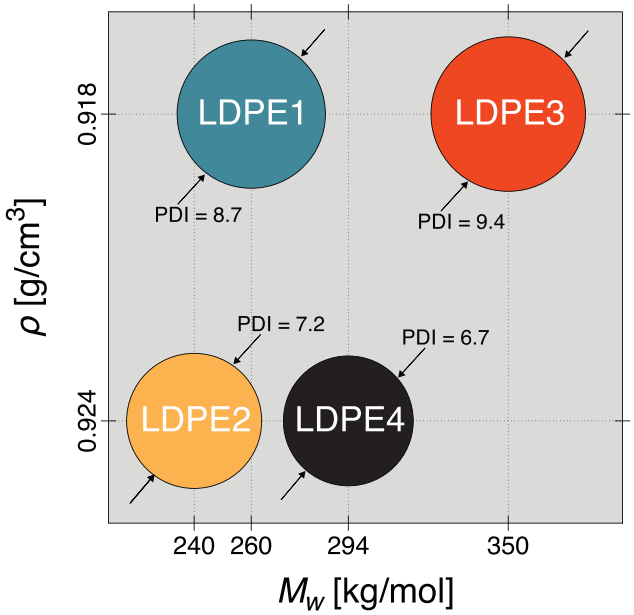

Figure 2. Bubble-chart graphical summary of the low-density polyethylenes investigated in this study, LDPE1-4, and how they can reveal the influence of molecular weight, M_w, and long-chain branching, LCB, on melt flow extrusion instabilities. The size of the bubbles is scaled with the polydispersity index, PDI.

four LDPEs cover in a brief manner the influence of both molecular weight and long-chain branching, Figure 2. We note that while the PDI varies between the low LCB and high LCB pairs, the differences are not considered as significant. Shear and extensional rheological properties are used to confirm the materials selection process later in the Section 3.

2.2. Characterization

The polymers were rheologically characterized in shear and extension using rotational and capillary rheometry. The testing temperature corresponded to the processing temperature, 140 °C.

An Anton Paar MCR702e Space rotational rheometer (Graz, Austria), in (twin-drive) separate motor–transducer configuration, equipped with a CTD450 convection oven was used for oscillatory shear tests. The measuring geometry was a 25 mm diameter parallel-plate used in counter-oscillation mode with a 1 mm gap. Based on linear viscoelastic regime limits determined from strain sweep tests (not shown), linear viscoelastic (small amplitude oscillatory shear) frequency sweep tests were performed in the angular frequency range of $\omega \in [10^{-2}, 4 \times 10^{2}]$ rad s^{-1} at a constant strain amplitude of 0.1%. The viscosity functions were fitted with the Carreau–Yasuda (four-parameter) model

$$\frac{|\eta(\omega)|}{|\eta_0|} = (1 + \tau_{CY}\omega^{a})^{\frac{n-1}{a}} \quad (1)$$

where $|\eta_0|$ is the zero-shear complex viscosity magnitudes and τ_{CY}, a, n are the characteristic relaxation time of the model and two other fit parameters.

Extensional rheological properties were determined using a universal extensional fixture (UXF). Samples of 0.5 mm thickness and 10 mm width were prepared by compression molding. The active measuring length was 19 mm. The transient uniaxial extensional viscosity, $\eta_E^+(t, \dot{\varepsilon})$ was measured at several Hencky strain rates, $\dot{\varepsilon} = 0.01, 0.03, 0.1, 0.3, 1, 3, 10$ s^{-1}. The steady state value thereof defines the extensional viscosity, that is, $\eta_E(\dot{\varepsilon}) = \lim_{t\to\infty}\eta_E^+(t, \dot{\varepsilon})$. The linear viscosity envelope (LVE), $\eta_E^0(t)$, was determined based on oscillatory shear data via the Cox–Merz rule.[31] The maximal strain hardening factors (SHF) were then determined for each polymer as

$$\mathrm{Max}\{\mathrm{SHF}(t, \dot{\varepsilon})\} = \frac{\mathrm{Max}\{\eta_E^+(t, \dot{\varepsilon})\}}{\eta_E^0(t)} \quad (2)$$

Steady shear viscosity functions were determined using a Goettfert RG20 capillary rheometer (Buchen, Germany) with a 30/1 (length/diameter) cylindrical measuring die.

For scanning electron microscopy (SEM) analysis, samples were first gold-sputtered and then visualized using a Philips XL-30 ESEM (Eindhoven, Netherlands).

2.3. Single Screw Extrusion

The extrusion experimental setup, **Figure 3**, consisted of a single-screw Brabender 19/25D (Duisburg, Germany) extruder (1) using a standard 2:1 compression screw and a custom slit die.[32,33] The slit die (11) had a straight flow channel of (length × width × height) of (132 × 20 × 2) mm. A conveyor belt (2) was placed after the die. The four heating zones of the extrusion setup, three along the extruder barrel and one at the die, were all set to the testing temperature, 140 °C. The extrusion temperature was kept intentionally low to facilitate the appearance of melt instabilities. Preliminary tests were performed up to 160 °C on two samples with similar results (data not shown). The melt pressure was monitored using two melt-pressure transducers (3 and 4), Terwin 2000 series (Nottingham, UK), max 700 bar, positioned at the extruder end and along the die. We briefly note that while the single-screw extruder setup used is certainly a greater experimental challenge compared to capillary rheometry based extrusion that the vast majority of similar studies use, it could be argued that the results are more relevant to polymer processing operations because they include the homogenization effects of the melting and metering regions of the screw.

Two types of test were performed: constant screw speed, mainly for validating the analysis method, and ramped screw

© 2023 The Authors. Macromolecular Materials and Engineering published by Wiley-VCH GmbH

14392054, 0, Downloaded from https://onlinelibrary.wiley.com/doi/10.1002/mame.202300088 by Karlsruher Inst F. Technologie, Wiley Online Library on [06/07/2023]. See the Terms and Conditions (https://onlinelibrary.wiley.com/terms-and-conditions) on Wiley Online Library for rules of use; OA articles are governed by the applicable Creative Commons License

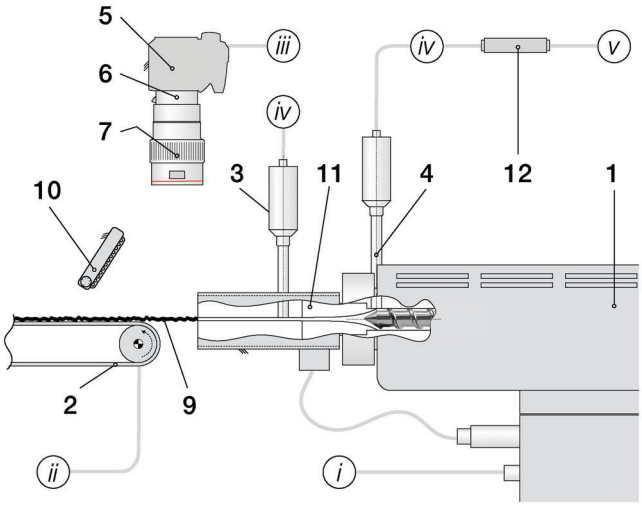

Figure 3. Schematic of the extruder and inline optical image system: (1) single screw extruder, (2) conveyor belt, (3,4) melt pressure transducers, (5, 6, 7) inline optical imaging system, (10) LED illumination system, (11) custom slit die and (12) National Instruments data acquisition board (pressure). Connectors (i–v) refer to the conveyor belt control connections and imaging and pressure data acquisition systems.

speed experiments to investigate MFEI spectral dynamics. The screw speed (n) was set from 0.1–150 rpm with a ramp rate of 0.1 rpm s^{-1}, the lowest ramp rate allowed by the instrument controller. It should be noted that while all experiments were run until 150 rpm, data recording was usually stopped at 100 or 120 rpm as (manual) feeding problems sometimes plagued the higher speeds. In addition, with the notable exception of LDPE4, which was run until 120 rpm, no further changes in the instability modes were observed past the data recording limit. The screw speed can be converted into the apparent shear rate inside the extrusion die, based on volumetric flow rate conservation between the metering region of the screw and the die, as [32,33]

$$\dot{\gamma} = \frac{6Q}{WH^2} = \frac{6(v_z W_s H_s)}{WH^2} = \frac{6[(\pi \cdot D \cdot n \cdot \cos\phi) W_s H_s]}{WH^2} \quad (3)$$

where W and H are the width and height of the slit die, respectively, Q is the volumetric flow rate, W_s, and H_s are the width and height of the screw in the metering zone, v_z is the normal average velocity inside the extrusion channel, and D, ϕ are the diameter of the screw in the metering zone and the helix angle, respectively. It should be noted that to simplify the notation, the apparent shear rate is written simply as $\dot{\gamma}$. The Weissenberg (Wi) number was then computed as

$$\mathrm{Wi} = \dot{\gamma}_a \tau \quad (4)$$

where τ is a characteristic polymer relaxation time that was taken based on the crossover in dynamic moduli, $\tau = \omega^{-1}|_{G'=G''}$, from oscillatory shear frequency sweep data, see also Table 1. As a rule-of-thumb for the present study, time (seconds) can be approximated into the screw speed (rpm) as $n \cong t \cdot 0.1$ and the screw speed (rpm) into apparent shear rate as $\dot{\gamma} \cong n \times 2.16$.

2.4. Inline Optical Imaging and Spectral Analysis

A Canon 60D EOS DSLR (Tokyo, Japan) camera (5) equipped with a 25 mm Canon extension tube and a 100 mm Canon L-series macro lens, was positioned 40 cm above the die exit. The camera system was complemented by an LED lighting system (10). Thus, the extrudate surface was recorded in high definition (HD) at a frame rate of 60 frames-per-second (fps). The video recordings were converted into space–time diagrams by appending a set line of pixels from each frame of the movie recording to a newly constructed image,[24,33–35] a common technique especially in fluid mechanics.[36] Therefore, this newly-constructed image (exemplified later in the manuscript) has the y-axis (ordinate) corresponding to the direction of the line of pixels chosen, while the x-axis (abscissa) will have effectively dimensions of time because the pixel lines are extracted from each successive movie frame. The distance between two consecutive pixels on the x-axis therefore corresponds to 1/60 s. While the temporal sensitivity of the inline optical method is significantly limiting compared to, for example, high sensitivity pressure-based systems, based on preliminary data,[12,34] a Nyquist frequency of 30 Hz was more than adequate to capture the MFEI expected in LDPEs while at the same time enabling a high-quality inline visual observation thereof.

Space–time images can be converted further into grayscale intensity data averaged along the extrudate width with a moving window procedure, and can be visualized in the frequency domain via Fourier-transformation in the form of spectrograms. The Fourier transform of a grayscale intensity function $g_j(t)$ is

$$G_j(t) = \int_{-\infty}^{\infty} g_j(t) e^{-i\omega \cdot t} \mathrm{d}t \quad (5)$$

where t is the time along the x-direction of the moving window j along a space–time diagram. An illustration of the moving window procedure and construction of the spectrograms is shown in **Figure 4**. The size of the moving window was 500 pixels which corresponds to 8.3 s. The size of the moving window was chosen to provide sufficient frequency resolution. The corresponding Fourier spectra (red highlights) can be converted into a grayscale colormap representation corresponding to time t_j. The window was then moved by 6 pixels (0.1 s) and the process was repeated corresponding to time $t_{j+1} = t_j + 0.1$ s. A certain degree of spectral leakage is expected, however, the size of the moving window increment ensures that such effects are minimal within the experimental timescale.

3. Results and Discussion

3.1. Rheological Characterization

Complex viscosity magnitude functions, $|\eta^*|(\omega)$, from oscillatory shear tests and steady shear apparent viscosity functions, $\eta_a(\dot{\gamma})$, are compared in **Figure 5**a. The data was also fitted with the Carreau–Yasuda model, Equation (1). The corresponding fit parameters can be found in Table S1, Supporting Information. The zero-shear viscosity, η_0, essentially confirms the relative difference in MFR between the samples as reported by the manufacturer: (LDPE3–LDPE4) have similar η_0, whereas (LDPE1–LDPE2)

© 2023 The Authors. Macromolecular Materials and Engineering published by Wiley-VCH GmbH

14392054, 0, Downloaded from https://onlinelibrary.wiley.com/doi/10.1002/mame.202300088 by Karlsruher Inst F. Technologie, Wiley Online Library on [06/07/2023]. See the Terms and Conditions (https://onlinelibrary.wiley.com/terms-and-conditions) on Wiley Online Library for rules of use; OA articles are governed by the applicable Creative Commons License

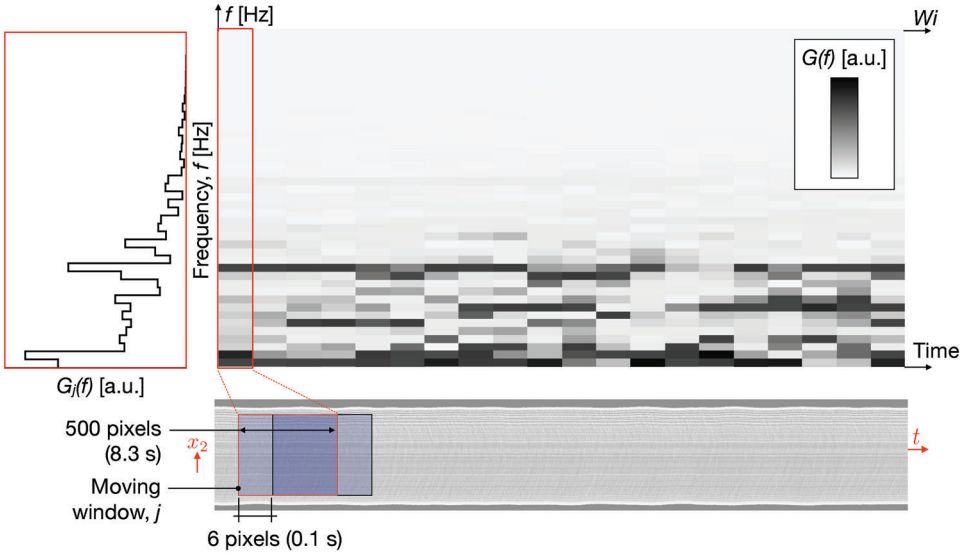

Figure 4. Qualitative illustration of the moving window procedure for obtaining spectrograms from space–time diagrams. The data is fictional.

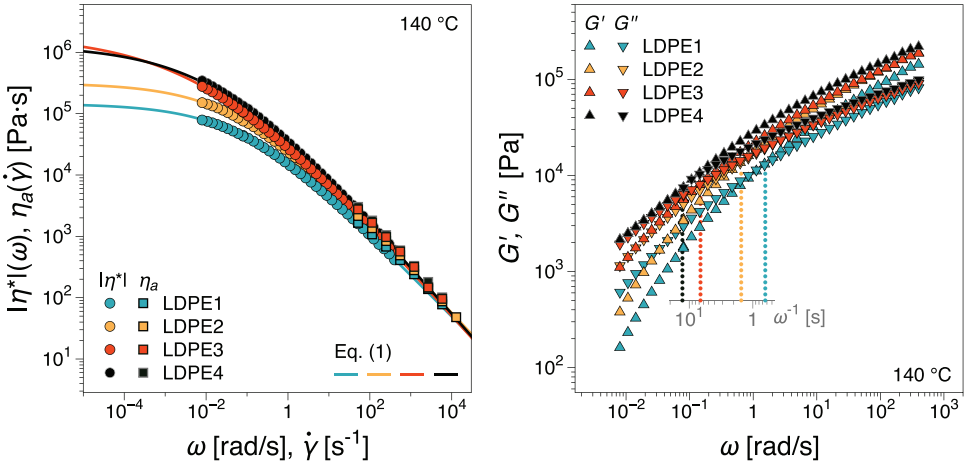

(a) (b)

Figure 5. Shear rheological properties of the polymer samples investigated: a) comparison between the complex viscosity magnitude, $|\eta^*|(\omega)$, from oscillatory shear frequency sweeps and steady shear apparent viscosity, $\eta_a(\dot{\gamma})$, testing the validity of the Cox–Merz rule and b) dynamic moduli, storage G' and loss G'' moduli, from oscillatory shear frequency sweeps. The inset axis in (b) represents the dynamic moduli crossover on a ω^{-1} scale.

are lower in agreement with their respective MFR. In nonlinear conditions above $\dot{\gamma} = 50\ s^{-1}$ the complex viscosity magnitude functions are nearly identical and correspond reasonably well to capillary rheometry data, confirming the validity of the Cox–Merz rule, in the respective shear rate range. Dynamic moduli as function of angular frequency are shown in Figure 5b. The crossover relaxation times are specified in the inset coordinate axis that corresponds to $[1/\omega]$.

The extensional viscosity of the polymers, **Figure 6**, emphasizes a similar behavior, with pairs (LDPE1–LDPE2) and (LDPE3–LDPE4) having similar η_E $(t \to \infty)$. Based on the maximal strain hardening factor, Equation (2), see **Figure 7**, pairs (LDPE1–LDPE3) and (LDPE2–LDPE4) suggest a very similar level of LCB increasing from the second to the first pair, confirming the sample overview in Figure 2.

3.2. Extrusion Instabilities and Spectral Analysis

3.2.1. Constant Screw Speed Pre-Tests

An example of an inline optical image visualization (frame extracted from the video recordings) is shown in **Figure 8** for LDPE4. Line L_1 marked in the figure corresponds to the line of pixels extracted from each frame for the construction of space–time plots. Based on the coordinate system in the figure, we refer to the space–time plots based on L_1 as (x_2, t). To exemplify the spectral analysis of the extrudates, we consider a series of experiments at several constant screw speeds without the moving window procedure, **Figure 9**. The (x_2, t) diagrams are shown in Figure 9a. Figure 9b contains the time-dependent grayscale intensity, $g(t)$, of the space–time diagrams. The grayscale

© 2023 The Authors. Macromolecular Materials and Engineering published by Wiley-VCH GmbH

14392054, 0, Downloaded from https://onlinelibrary.wiley.com/doi/10.1002/mame.202300088 by Karlsruher Inst F. Technologie, Wiley Online Library on [06/07/2023]. See the Terms and Conditions (https://onlinelibrary.wiley.com/terms-and-conditions) on Wiley Online Library for rules of use; OA articles are governed by the applicable Creative Commons License

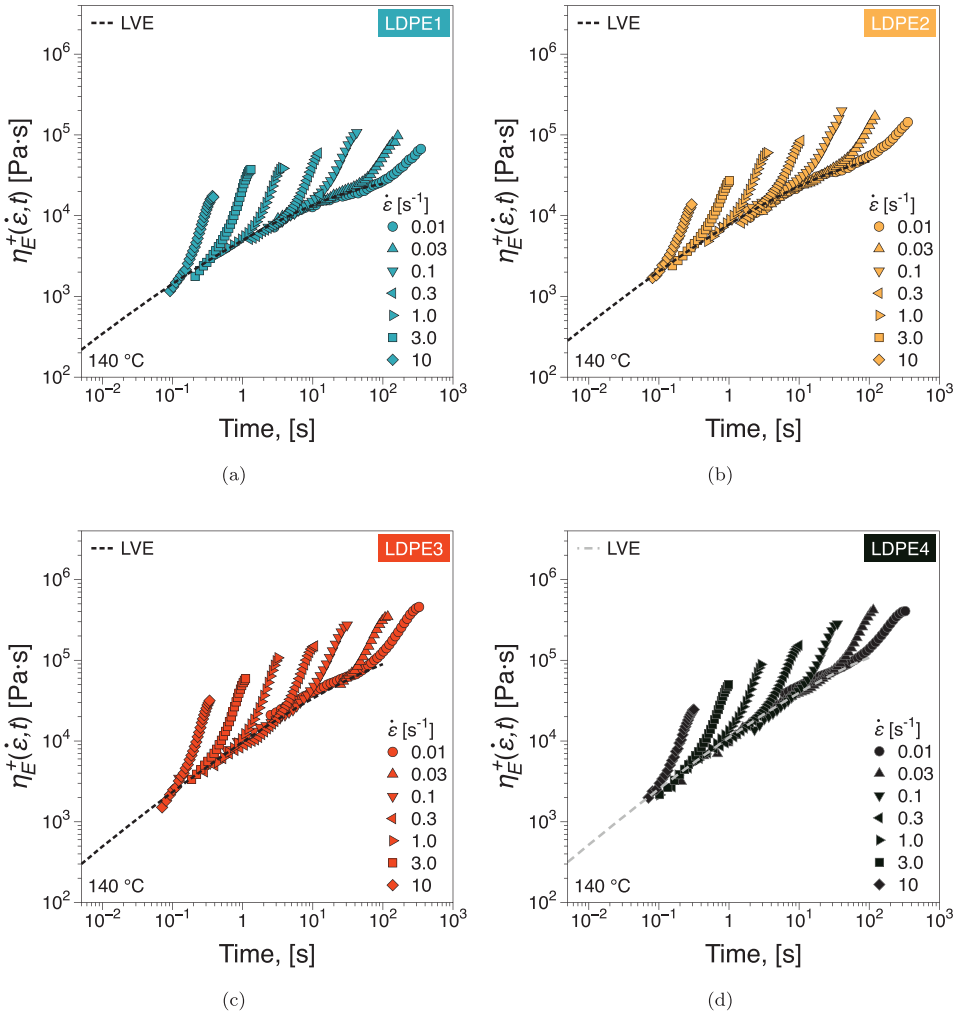

Figure 6. Transient extensional viscosity functions, $\eta_E^+(\dot{\epsilon}, t)$, for a range of imposed Hencky strain rates, $\dot{\epsilon}$: a) LDPE1, b) LDPE2, c) LDPE3, d) LDPE4. LVE is the linear viscoelastic envelope.

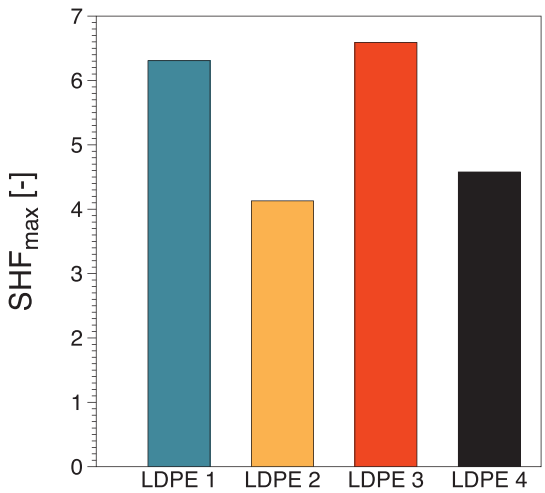

Figure 7. Maximal strain hardening factor (SHF_{max}) based on the transient extensional data in Figure 6.

intensity plotted was averaged along the extrudate width (x_2 direction). The data is presented in the frequency domain, $G(t)$, via Fourier-transformation in Figure 9c.

As the screw speed increases from the bottom to the top diagrams, the rotational frequency of the screw, f_n, can be first identified together with several of its higher harmonics $i \times f_n$, $i = 1$, 2, 3.... In addition, we detect an additional peak in the Fourier spectra that corresponds to the surface patterns evidenced by the space–time diagrams in Figure 9 f_{ch1}, up to $n = 50$ rpm. We briefly note that at a first observation $n = 20$ rpm has a distinctly broader characteristic frequency peak. For $n = 102$ rpm, low frequency distortions in the extrudate can be observed for $n = 102$ rpm in Figure 9a. Thus, two characteristic pattern peaks can be identified in the Fourier spectrum. One is $f_{ch1} \cong 6$ Hz and a small low frequency peak at $f_{ch2} \cong 1.7$ Hz. It is important to note that the frequency of the screw at 102 rpm corresponds also to 1.7 Hz. The pattern frequencies have been manually verified from the space–time images to confirm that $f_{ch2} \cong f_n$. The implications thereof are discussed further in the manuscript. Thus, surface extrudate

© 2023 The Authors. Macromolecular Materials and Engineering published by Wiley-VCH GmbH

14392054, 0, Downloaded from https://onlinelibrary.wiley.com/doi/10.1002/mame.202300088 by Karlsruher Inst F. Technologie, Wiley Online Library on [06/07/2023]. See the Terms and Conditions (https://onlinelibrary.wiley.com/terms-and-conditions) on Wiley Online Library for rules of use; OA articles are governed by the applicable Creative Commons License

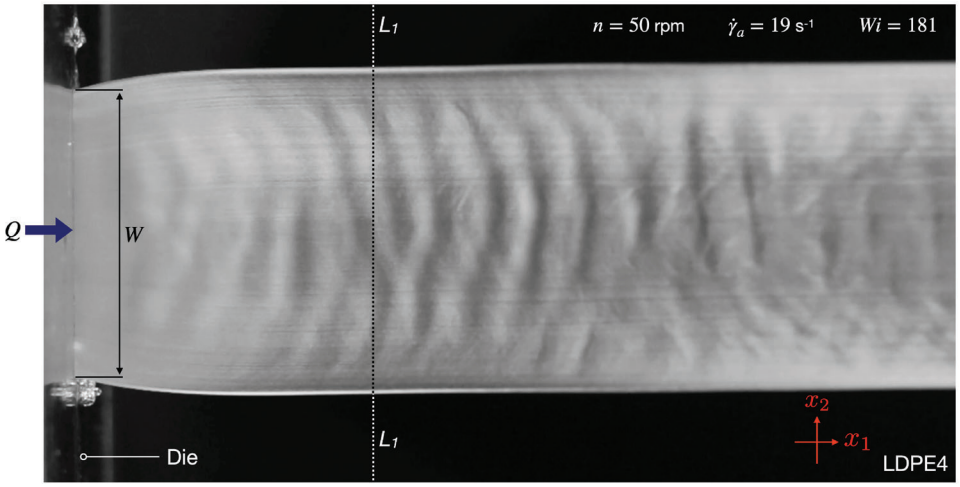

Figure 8. Example of surface distortions as viewed inline (single frame from video recording) through the optical visualization setup (LDPE4 at 140 °C). Line L_1 represents the line of pixels extracted from video frames to construct (x_2, t) space–time diagrams.

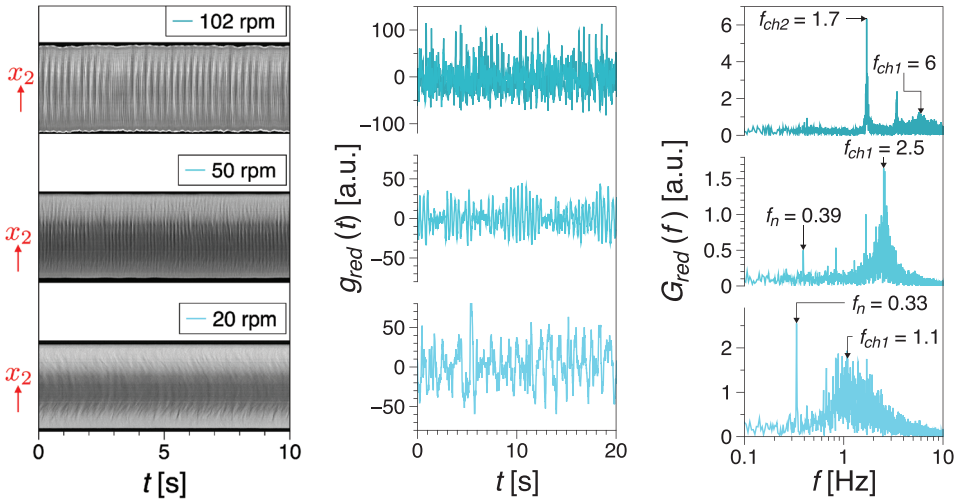

Figure 9. Example of extrusion flow progression with increasing apparent shear rate (screw speed): a) (x_2, t) space–time diagrams, b) reduced gray intensity in the time domain, $g_{red}(t)$ and c) reduced gray intensity in the frequency domain via Fourier-transform analysis, $G_{red}(\omega)$. Data was obtained using LDPE4.

patterns at $n = 102$ rpm are defined by two characteristic frequencies, $f_{ch1,\,2}$, that is, $\#f_{ch} = 2$.

3.2.2. Ramped Screw Tests

To determine the full spectrum of MFEI in relation to the molecular weight, M_w, and long-chain branching, LCB, of the polymers we performed ramped screw speed experiments and the data was analyzed in the manner exemplified in Figure 9. It should be noted that while ideally the aim was to perform quasi-steady-state tests, due to the long polymer relaxation times the tests are likely in transient state. However, the goal of the ramped experiments was to have a facile overview of all the surface patterns that could be identified for each LDPE, that is, their sequence of instabilities. Space–time diagrams corresponding to the ramped tests are presented in **Figure 10**. For reference, the pressure measured by the transducer placed along the die, (3) in Figure 3, during the tests is shown in Figure S1, Supporting Information. We note that pressure data acquired at high data acquisition rates from the transducer were also examined through Fourier-transform analysis (data not shown), however, at least at that distance from the die exit no instabilities could be detected therein, in agreement with similar results.[12] Two aspects are important to consider based on a qualitative inspection of the space–time plots. First, at low Wi (shear rates or screw speeds) it was difficult to position the extrudate between die and conveyor belt.[33] Second, because we selected a low

© 2023 The Authors. Macromolecular Materials and Engineering published by Wiley-VCH GmbH

14392054, 0, Downloaded from https://onlinelibrary.wiley.com/doi/10.1002/mame.202300088 by Karlsruher Inst F. Technologie, Wiley Online Library on [06/07/2023]. See the Terms and Conditions (https://onlinelibrary.wiley.com/terms-and-conditions) on Wiley Online Library for rules of use; OA articles are governed by the applicable Creative Commons License

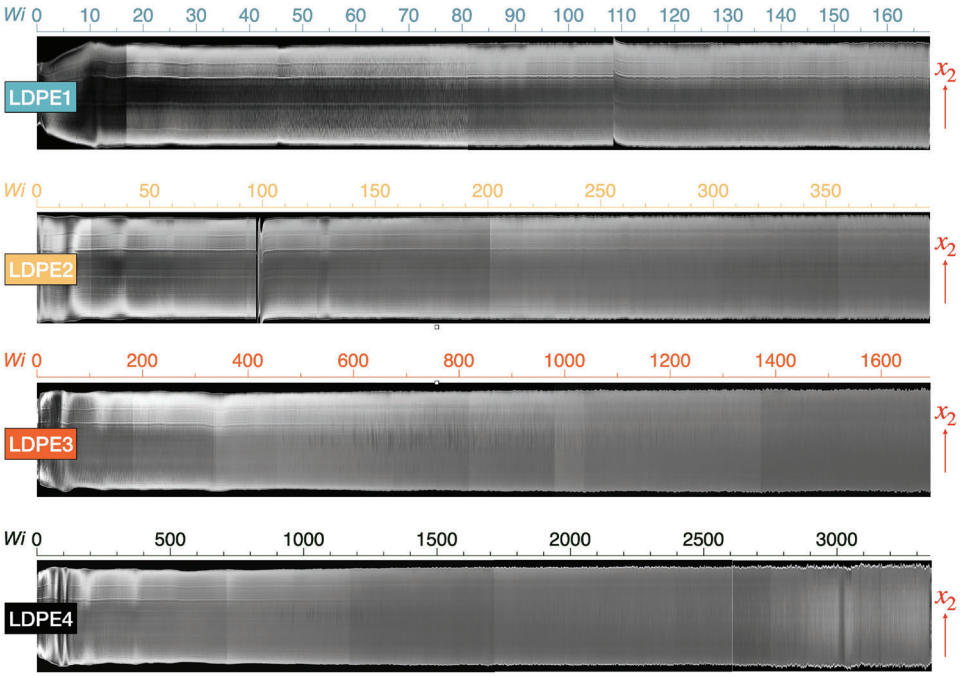

Figure 10. Space–time diagrams, (x_2, t) from inline optical imaging as function of time and Wi during ramped screw speed experiments.

temperature for the extrusion experiments to trigger the onset of instabilities as early as possible, it is clear from the visualizations that surface patterns are already present on the extrudates at the lowest Wi.

While such temperatures are likely unrealistic for the vast majority of polymer processing operations, we emphasize again that the goal of the study is to determine whether there are any specific surface pattern transition sequences that characterize long-chain branched polymers.

The spectral analysis corresponding to the space–time diagrams in Figure 10 is presented in the form of spectrograms in **Figure 11**. The spectrograms represent the evolution of $G_j(t)$, Equation (5) in the frequency domain (ordinate) as function of Wi or time (abscissa), where the intensity of the colormap corresponds to the magnitude of $G_j(t)$. Additionally, to provide a complete picture of the surface morphology of the investigated extrudates, SEM visualizations of the extrudates at the highest screw speed or Wi are shown in Figure S2, Supporting Information. Interestingly, based on their appearance, for LDPE1, LDPE, and LDPE3 they could be perhaps considered to be "sharkskin"-like surface features at lengthscales well below what the inline optical system could detect.

For the low M_w—high LCB LDPE1, Figure 11a very weak surface patterns can be distinguished for Wi > 6.5 that appear rather irregular, see detail A. This translates in relatively broad characteristic spectral peaks, see f_{ch1}. As it can be observed in the A and B visual details, A–B, the surface patterns continue to be rather irregular and exhibit a form of 'criss-cross' surface patterns (CCSP). Evidence of a similar patterns in the scientific literature could perhaps be inferred for the LCB in Filipe et al.,[21] see Figure 4 in their publication.[21] In addition to the broad CCSP pattern characteristic frequency, the onset of a narrow peak at higher frequency can be readily observed. However, the only pattern features that correspond to that particular frequency range are oscillations on scratches present on the surface of all extrudates in the form of a continuous narrow band at fixed x_2 (artifact).

For the low M_w—low LCB LDPE2, Figure 9b, with increasing Wi we identified f_{ch1} to correspond the CCSP, see details A, B in the figure. In contrast to LDPE1, around Wi≅225, f_{ch1} converts into a narrower higher-intensity peak corresponding to clearly-defined ripples on the extrudate, MFEI that we called surface ripples (SR). These are essentially identical patterns to those obtained by Georgantopoulos et al.,[24] see, for example, Figure 13 in the respective publication.[24] Similar patterns could also have been observed by Filipe et al.,[21] see LCB6 in Figure 4 in their publication, however, it would appear that it was part of a stick-slip MFEI.[21] We note also that f_{ch1} recorded at the highest Wi are higher than for LDPE1. The lower peak detected at approximately Wi = 285 appears to be likely correlated to similar scratch-artifacts as described for LDPE1, or to sub-harmonics of f_{ch1}.

For the high M_w—high LCB LDPE3, Figure 11c, the MFEI transition sequence starts also with CCSP, see detail A. However, it is not entirely clear if the pattern does not represent actually a transition state from CCSP to SR, as could be inferred when examining the core region of the extrudate that appears to resemble SR to a certain extent. Well-developed SR can be distinguished for approximately Wi > 70 with a clearly distinguishable higher harmonic of f_{ch_1}. Interestingly, small low frequency surface extrudate distortions can be distinguished for Wi > 550, see detail C. These are difficult to identify in the spectrograms due to the decay of intensity in the spectra at low frequencies, see f_{ch2}. Thus, we propose that for LDPE3, SR transitions to a new pattern that consists of the superposition of two frequencies, that is, superimposed ripples (SiR), see the darker periodic features in detail C. The amplitudes of the low frequency distortions are smaller

© 2023 The Authors. Macromolecular Materials and Engineering published by Wiley-VCH GmbH

14392054, 0, Downloaded from https://onlinelibrary.wiley.com/doi/10.1002/mame.202300088 by Karlsruher Inst F. Technologie, Wiley Online Library on [06/07/2023]. See the Terms and Conditions (https://onlinelibrary.wiley.com/terms-and-conditions) on Wiley Online Library for rules of use; OA articles are governed by the applicable Creative Commons License

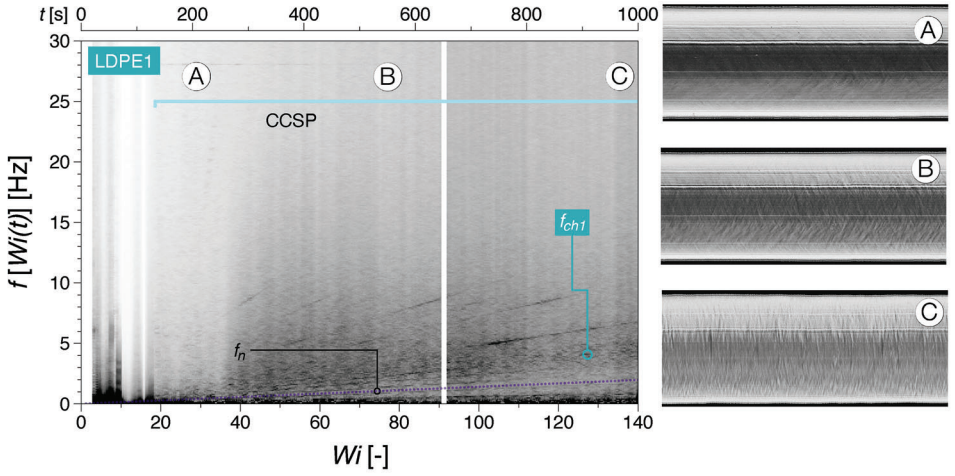

(a)

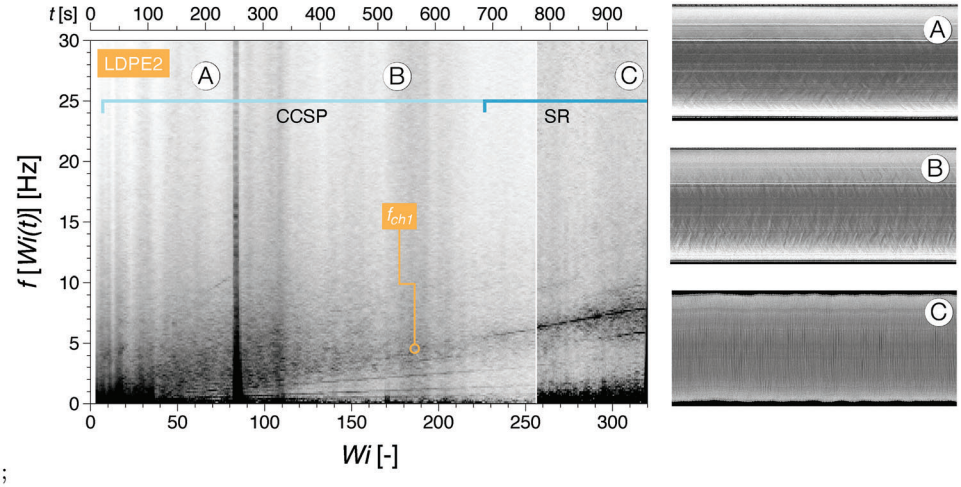

(b)

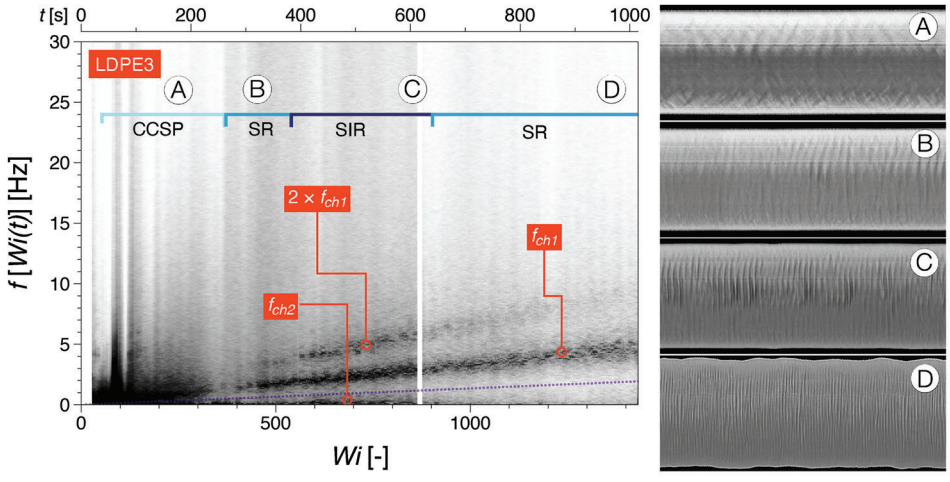

(c)

Figure 11. Spectrograms, diagrams showing the evolution of the frequency spectra associated to the extrudate surface as a function of time, see also Figure 4, for a) LDPE1, b) LDPE2, c) LDPE3, and d) LDPE4. Images on the right side are corresponding sections from the space–time plots in Figure 10. Notations: CCSP - criss-cross surface patterns; SR - surface ripples; SiR - superimposed ripples.

© 2023 The Authors. Macromolecular Materials and Engineering published by Wiley-VCH GmbH

14392054, 0, Downloaded from https://onlinelibrary.wiley.com/doi/10.1002/mame.202300088 by Karlsruher Inst F. Technologie, Wiley Online Library on [06/07/2023]. See the Terms and Conditions (https://onlinelibrary.wiley.com/terms-and-conditions) on Wiley Online Library for rules of use; OA articles are governed by the applicable Creative Commons License

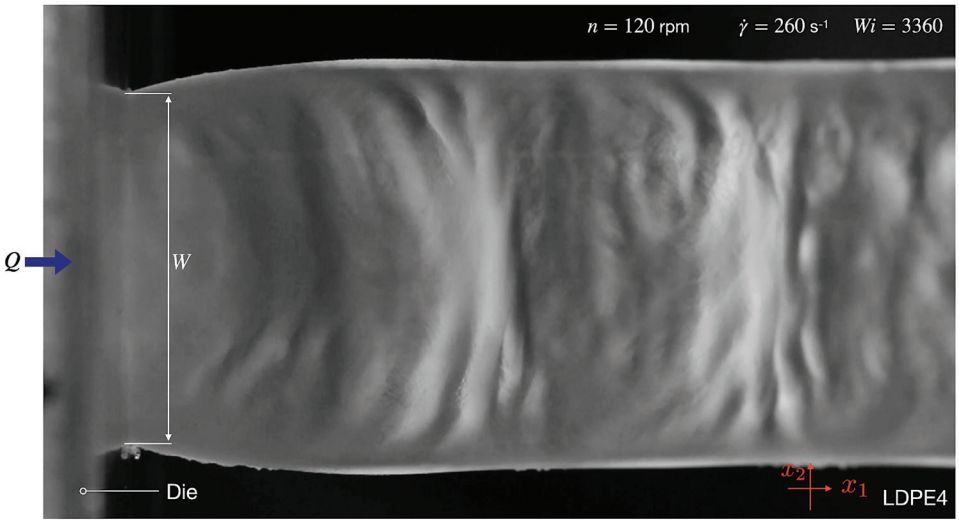

Figure 12. Optical visualization (single frame from video recording) of melt flow instabilities characterized by two superimposed characteristic frequencies, that is, SiR-v (Superimposed Ripples) in the form of volume distortions, in LDPE4.

than the extrudate thickness and thus SiR in LDPE3 can be classified as a surface MFEI, SiR-s. This type of low frequency superposition is similar to that observed by Kádár et al.,[12] using capillary rheometry, however, we note that the surface patterns therein observed were considerably more distorted.[12] We also note that some additional noise in the low frequency region of the spectra coupled with potentially similar low frequency events could be inferred for LDPE2 as well, however, the surface distortions appeared rather irregular and lower than can be distinguished within the moving widow number of points (see detail C). Rather surprisingly, in LDPE3 the low frequency component of the pattern was eliminated with increasing Wi, with the MFEI reverting to SR above approximately Wi > 910. see detail D.

For the high M_w, low LCB LDPE4, Figure 11d, the succession of instabilities is similar to LDPE3, starting with CCSP, see detail A, that quickly transitions to SR at approximately Wi > 880. Some low frequency irregular surface distortions could potentially have appeared already in the SR region, however, with no clear evidence thereof in the spectra. Interestingly, for Wi > 2950 a very pronounced SiR MFEI type was recorded, see detail C. Being characterized by a higher f_{ch2} (approximately 1.2 Hz) compared to LDPE3 (approximately 0.5 Hz) this SiR pattern resulted in a pronounced volume distortion, that is, SiR-v, as the amplitude of f_{ch2} was comparable to the thickness of the extrudate, see also the single frame in **Figure 12**. Such volume distortions with $\#f_{ch} = 2$ have previously been reported by Kádár et al.,[12] however their patterns appeared to be more distorted. It is important at this stage to consider the influence of the screw rotation frequency on the development of instabilities. Already in Figure 9c we identified the characteristic f_{ch2} to coincide with f_n and we note again that the pattern characteristic surfaces have been manually verified from the space–time diagrams. The data in Figure 11d confirms this occurrence. Thus, it would appear that especially the SiR-v instabilities are susceptible to mechanical perturbations, that is, vibrations, and thus there appears to be a frequency lock-in effect of f_{ch2} with f_n. However, we note that previous observations of SiR-v have been made using capillary rheometers. Therefore, we conclude that likely SiR is the result of an intrinsic polymer MFEI susceptibility to the superposition of a low surface or volume extrudate distortion on SR. This could be triggered by mechanical disturbances and, in the case of single-screw extruders, the rotational frequency of the screw plays a determinant role.

The characteristic frequencies and wavelengths of the instabilities of each LDPE and the associated patterns are summarized in **Figure 13** as function of Wi. The points were extracted manually from spectra at selected Wi from the spectrograms in Figure 11. The error bars thus represent the widths of the peaks in the Fourier spectra while the plotted points represent the maximum of the peak, see also Figure 9c. Due to the use of Wi (scaled with τ in Table 1) as independent variable, the low M_w (LDPE1–LDPE2) are readily distinguished from the higher M_w pair (LDPE3–LDPE4) by approximately one order of magnitude in Wi-range. The characteristic frequency peaks can be fitted with a power function[27] of the form $f_{ch} = a \cdot \mathrm{Wi}^b$. A version of the figure where the apparent shear rate was used as independent variable, with fits included, can be found in Figure S3, Supporting Information. In this way the high LCB pair (LDPE1-LDPE3) share a common scaling behavior with slopes $b \cong 0.8$ while the low LCB pair (LDPE2-LDPE4) slightly higher slopes with $b^{LDPE2} = 1.2$ and $b^{LDPE3} = 0.9$. Therefore, for the lower M_w pair (LDPE1–LDPE3) with the transition to SR in LDPE2, the two polymers appear to converge in f_{ch1}. All slopes are considerably larger than those obtained for a similar LDPE[24] (0.3) as well as LLDPE (0.3) and styrene-butadiene rubbers.[16] This could be however more related to the different experimental protocols used, ramped versus steady state step-wise tests, rather than an influence of molecular properties.

The wavelength was calculated as $\lambda = \langle v_e \rangle / f_{ch}$, where $\langle v_e \rangle$ was determined based on space–time diagrams using a procedure described elsewhere.[37] The wavelength distribution (error bars) was not included to preserve clarity. Interestingly, the characteristic wavelengths are corresponding to all instability types are very similar and appear to be constant or decreasing with

© 2023 The Authors. Macromolecular Materials and Engineering published by Wiley-VCH GmbH

14392054, 0, Downloaded from https://onlinelibrary.wiley.com/doi/10.1002/mame.202300088 by Karlsruher Inst F. Technologie, Wiley Online Library on [06/07/2023]. See the Terms and Conditions (https://onlinelibrary.wiley.com/terms-and-conditions) on Wiley Online Library for rules of use; OA articles are governed by the applicable Creative Commons License

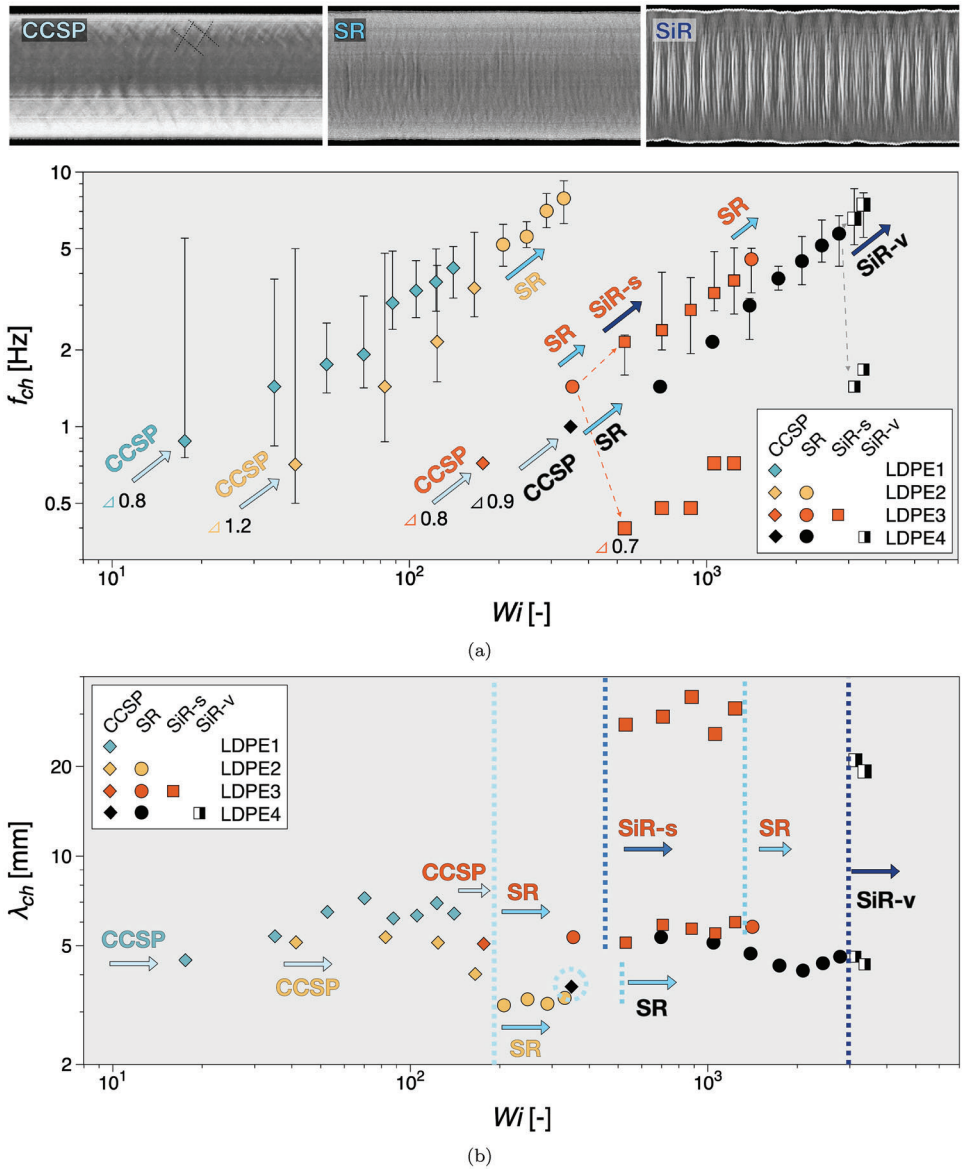

Figure 13. Stability diagrams showing a) the characteristic frequencies and (b) characteristic wavelengths associated to melt flow instabilities in the LCB polymers investigated in this study as function of the Weissenberg number, Wi. The error bars approximate the width of the characteristic frequency peak, see also Figure 9. Notations: CCSP - criss-cross surface patterns; SR - surface ripples; SiR - superimposed ripples that can be surface (-s) or volumetric (-v) instabilities. Characteristic wavelength broadness (error bars) have been removed for clarity.

increasing Wi. This is in contrast with the expected increase with increasing Wi (shear rate).[24,35] This could be attributed once again to the ramped experimental protocol used in this study. The decreases in λ_{ch1}, see LDPE2 at the transition to SR and LDPE4 at the transition to SiR-v and could be potentially attributed to wall slip behavior. Interestingly, a criterion for the onset of SR could be inferred for LDPE1–LDPE3 at $Wi_{cr1} \approx 190–220$. In this case, the LDPE4 SSCP regime could then be a transition regime between CCSP and SR. Thus for $Wi < Wi_{cr1}$ the instability types are CCSP while for $Wi > Wi_{cr_1}$ there is a broad transition to SR and / or SiR, with the higher M_w polymers being more susceptible to SiR-s for higher LCB and to SiR-v for the lower LCB polymers.

Thus, we can summarize that three distinct surface patterns could be identified in the long-chain branched polyethylenes analyzed. The primary MFEI exhibited by LDPE1–LDPE4 could be defined as:

- CCSP (criss-cross surface pattern), Figure 13 top-left; $\#f_{ch} = 1$; broad low-intensity characteristic frequency; surface MFEI.

LDPE2–LDPE4 all showed surface ripples defined as:

- SR (surface ripples), Figure 13 top-middle; $\#f_{ch} = 1$; narrower characteristic frequency and higher intensity compared to CCSP; surface MFEI.

© 2023 The Authors. Macromolecular Materials and Engineering published by Wiley-VCH GmbH

14392054, 0, Downloaded from https://onlinelibrary.wiley.com/doi/10.1002/mame.202300088 by Karlsruher Inst F. Technologie, Wiley Online Library on [06/07/2023]. See the Terms and Conditions (https://onlinelibrary.wiley.com/terms-and-conditions) on Wiley Online Library for rules of use; OA articles are governed by the applicable Creative Commons License

LDPE3 and LDPE4, both having the highest molecular weights, showed a third instability type characterized by a superposition of two characteristic frequencies, with patterns varying from surface (LDPE3) to volume (LDPE4) extrudate distortions:

- SiR (superimposed ripples), see Figure 13 top-right; $\#f_{ch} = 2$; weak SiR thereof constitute surface distortions, that is, SiR-s; when fully developed they are volume distortions, that is, SiR-v.

4. Conclusions

Melt flow extrusion instabilities (MFEI) in long-chain branched polymers have been studied from an extrudate pattern point of view using inline image analysis. To the extent of our knowledge, this is the first study to address this particular aspect of MFEI. The four low-density polyethylenes (LDPEs) were selected to cover both the influence of average molecular weight (M_w) and long-chain branching (LCB), material selection confirmed by the shear and extensional rheological behavior of the polymers. Despite usually not being the focus of MFEI studies in polymer melts, the LCB PEs investigated showed three MFEI types that we consider distinct from the MFEI encountered in linear polymers: criss-cross surface patterns (CCSP), surface ripples (SR) and superimposed surface ripples (SIR). Both M_w and LCB had a significant effect on the MFEI transition sequences identified. Low M_w generally favored CCSP, a weak surface type of MFEI. When increasing M_w, the transition sequence was complex and involved all three MF types identified. For both lower and higher M_w LDPEs, LCB appeared to have a somewhat stabilizing effect on the transition sequences. For the high M_w pair (LDPE3-LDPE4), lower LCB in LDPE4 showed the most striking instability types, consisting of volume SiR-v, extrudate distortions albeit at very high Wi. By increasing LCB even for higher M_w, LDPE3 showed surface SiR, SiR-s, that although had their onset at lower Wi compared to LDPE4 they also disappeared with increasing *Wi* with the instability type reverting to SR. Therefore, we can infer that higher M_w generally promotes the onset of low frequency extrudate components. LDPE1 and LDPE2 likely contained the influence of both M_w and LCB as CCSP and SR were identified for LDPE2 while only CCSP for LDPE1.

Supporting Information

Supporting Information is available from the Wiley Online Library or from the author.

Acknowledgements

S.P., A.A., and C.K.G. contributed equally to this work. S.P. and R.K. are grateful to Arvindh Seshadri Suresh for his help in re-examining the extrudates. Authors thank the group of Prof. Markus Busch from TU Darmstadt with special recognition to Hans-Michael Orfgen for the support with GPC tests. Håkan Millqvist is acknowledged for manufacturing the custom extrusion die.

Conflict of Interest

The authors declare no conflict of interest.

Data Availability Statement

The data that support the findings of this study are available from the corresponding author upon reasonable request.

Keywords

inline imaging, long-chain branched polymers, melt flow instabilities, spectral analyses

Received: March 13, 2023
Revised: April 16, 2023
Published online:

[1] To avoid the classical confusion with the melt flow index, we refer to the latter by its alternative terminology, MFR - melt flow rate.
[2] M. Denn, *Annu. Rev. Mech.* **2001**, *33*, 265.
[3] C. J. S. Petrie, M. M. Denn, *AIChE J.* **1976**, *22*, 209.
[4] R. G. Larson, *Rheol. Acta* **1992**, *31*, 213.
[5] A. Leonov, A. Prokunin, *Nonlinear Phenomena in Flows of Viscoelastic Polymer Fluids*, Chapman & Hall, London **1994**.
[6] S. Hatzikiriakos, K. Migler, editors, *Polymer Processing Instabilities. Control and Understanding*, Marcel Dekker, New York City **2005**.
[7] P. G. Lafleur, B. Vergnes, *Polymer Extrusion*, Wiley-ISTE, New York **2014**.
[8] J.-F. Agassant, C. Combeaud, L. Robert, B. Vergnes, D. Arda, M. Mackley, A. Merten, H. Münstedt, *Int. Polym. Process.* **2006**, *21*, 239.
[9] J. Meissner, *Polym. Test.* **1983**, *3*, 291.
[10] I. F. C. Naue, Master's Thesis, TUD - Technical University Darmstadt, Darmstadt, **2007**.
[11] H. Palza, I. F. Naue, M. Wilhelm, *Macromol. Rapid Commun.* **2009**, *30*, 1799.
[12] R. Kádár, I. F. Naue, M. Wilhelm, *Polymer* **2016**, *104*, 193.
[13] M. Barczewski, R. Barczewski, T. Chwalczuk, *J. Manuf. Processes* **2020**, *59*, 153.
[14] E. Miller, J. P. Rothstein, *Rheol. Acta* **2004**, *44*, 160.
[15] A. Hammer, W. Roland, M. Zacher, B. Praher, G. Hannesschläger, B. Löw-Baselli, G. Steinbichler, *Polymers* **2021**, *13*, 17.
[16] C. K. Georgantopoulos, M. K. Esfahani, C. Botha, I. F. C. Naue, N. Dingenouts, A. Causa, R. Kádár, M. Wilhelm, *Macromol. Mater. Eng.* **2021**, *306*, 2000801.
[17] J. Perez-Gonzalez, L. Perez-Trejo, L. de Vargas, O. Manero, *Rheol. Acta* **1997**, *36*, 677.
[18] N. El Kissi, J.-M. Piau, F. Toussaint, *J. Non-Newtonian Fluid Mech.* **1997**, *68*, 271.
[19] O. Delgadillo-Velázquez, S. Hatzikiriakos, *Polym. Eng. Sci.* **2007**, *47*, 1317.
[20] T. Yoo, D. Kim, Y. Son, *J. Appl. Polym. Sci.* **2012**, *126*.
[21] S. Filipe, I. Vittorias, M. Wilhelm, *Macromol. Mater. Eng.* **2008**, *293*, 57.
[22] H. Palza, S. Filipe, I. F. Naue, M. Wilhelm, *Polymer* **2010**, *51*, 522.
[23] T. I. Burghelea, H. J. Griess, H. Münstedt, *J. Non-Newtonian Fluid Mech.* **2010**, *165*, 1093.
[24] C. K. Georgantopoulos, M. K. Esfahani, I. F. C. Naue, M. Wilhelm, R. Kádár, *J. Appl. Polym. Sci.* **2023**, *140*, e53165.
[25] C. den Doelder, Ph.D. Thesis, Eindhoven University of Technology, Eindhoven, **1999**.
[26] I. F. C. Naue, R. Kádár, M. Wilhelm, *Macromol. Mater. Eng.* **2015**, *300*, 1141.
[27] C. K. Georgantopoulos, M. K. Esfahani, C. Botha, M. A. Pollard, I. F. C. Naue, A. Causa, R. Kádár, M. Wilhelm, *Phys. Fluids* **2021**, *33*, 093108.

© 2023 The Authors. Macromolecular Materials and Engineering published by Wiley-VCH GmbH

14392054, 0, Downloaded from https://onlinelibrary.wiley.com/doi/10.1002/mame.202300088 by Karlsruher Inst F. Technologie, Wiley Online Library on [06/07/2023]. See the Terms and Conditions (https://onlinelibrary.wiley.com/terms-and-conditions) on Wiley Online Library for rules of use; OA articles are governed by the applicable Creative Commons License

[28] N. El Kissi, J. Paiu, *J. Non-Newtonian Fluid Mech.* **1990**, *37*, 55.
[29] N. E. Kissi, L. Léger, J.-M. Piau, A. Mezghani, *J. Non-Newtonian Fluid Mech.* **1994**, *52*, 249.
[30] J. Piau, N. El Kissi, B. Tremblay, *J. Non-Newtonian Fluid Mech.* **1990**, *34*, 145.
[31] H. Münstedt, F. R. Schwarzl, *Deformation and Flow of Polymeric Materials*, Springer, Berlin, Heidelberg **2014**.
[32] Y. L. Thadavathi, S. Wassén, R. Kádár, *J Food Eng.* **2019**, *245*, 112.
[33] S. Pashazadeh, R. Ghanbari, M. Bek, A. Aulova, T. Moberg, A. Brolin, R. Kádár, unpublished.
[34] R. Kádár, *Annu. trans. Nord. Rheol. Soc.* **2017**, *25*, 99.
[35] C. K. Georgantopoulos, M. K. Esfahani, M. A. Pollard, I. F. C. Naue, A. Causa, R. Kádár, M. Wilhelm, *Macromol. Mater. Eng.* **2022**, *307*, 2200313.
[36] R. Kádár, C. Balan, *Eur. J. Mech., B* **2012**, *31*, 158.
[37] S. Pashazadeh, A. S. Suresh, T. Moberg, A. Brolin, R. Kádár, unpublished.

© 2023 The Authors. Macromolecular Materials and Engineering published by Wiley-VCH GmbH

14392054, 0, Downloaded from https://onlinelibrary.wiley.com/doi/10.1002/mame.202300088 by Karlsruher Inst F. Technologie, Wiley Online Library on [06/07/2023]. See the Terms and Conditions (https://onlinelibrary.wiley.com/terms-and-conditions) on Wiley Online Library for rules of use; OA articles are governed by the applicable Creative Commons License